Electromagnetic and Mechanical Modeling of Medium Voltage PMSM for Hybrid Regional Aircraft in Faulty Conditions

Electromagnetic and Mechanical Modeling of Medium Voltage PMSM for Hybrid Regional Aircraft in Faulty Conditions

Paolo Pescetto
Dept. of Energy "Galileo Ferraris"
Politecnico di Torino, Torino, Italy
paolo.pescetto@polito.it

Federico Cocuzza
Dept. of Mech. and Aerospace Engineering
Politecnico di Torino, Torino, Italy
federico.cocuzza@studenti.polito.it

Fahimeh Mashayekhi
Dept. of Mech. and Aerospace Engineering
Politecnico di Torino, Torino, Italy
fahimeh.mashayekhi@polito.it

Simone Ferrari
Dept. of Energy "Galileo Ferraris"
Politecnico di Torino, Torino, Italy
simone.ferrari@polito.it

Stefano Zucca
Dept. of Mech. and Aerospace Engineering
Politecnico di Torino, Torino, Italy
stefano.zucca@polito.it

Christian Firrone
Dept. of Mech. and Aerospace Engineering
Politecnico di Torino, Torino, Italy
christian.firrone@polito.it

Gianmario Pellegrino
Dept. of Energy "Galileo Ferraris"
Politecnico di Torino, Torino, Italy
gianmario.pellegrino@polito.it

***Abstract*—This paper presents a comprehensive modeling approach for the propulsion system of a hybrid regional aircraft. The propeller rotation is guaranteed by the turbo engine and the electrical drive in a parallel architecture. The electric drive is coupled to the transmission system through an overrunning clutch, allowing the motor disengagement in the event of a fault or in specific phases during flight. The drive is powered by a 3-level medium voltage Active Neutral Point Clamped (ANPC) converter rated 2400 V. The model focuses on accurately simulating various faults in the drive, including 3-phase, single-phase, switch failures in the power converter, and open circuit faults. The developed model permits to evaluate the impact on the full propulsion system, including maximum transient current and torque, torque undulations, and potential clutch disengagement.**

***Index Terms*—More electric aircraft, Motor modeling, Hybrid propulsion systems, NVH, Safety critical applications, Fault analysis.**

I. Introduction

Numerous studies emphasize the urgent need to decarbonize global industries, including aviation. In response, significant public [1] and private investments have driven the development of innovative technologies to electrify aviation systems. The electrification process began with replacing auxiliary systems with electrical actuators. This trend was often referred to as More Electric Aircraft (MEA), and it permitted to reduce the aircraft weight and fuel consumption up to 9% and 8% respectively [2]–[4]. Today, advanced motor drives and power converters are paving the way to address one of the key challenges for hybrid avionic propulsion [5]. This poses serious challenges in the design and control of power converters [6], fault-tolerant electric motors [7]–[10] and on-board distribution system [11].

The avionic applications require extremely high power density [12], due to the limited available space onboard and to the severe increase of fuel consumption with the aircraft weight. In addition, a high efficiency is required [13] due to the difficulty of heat dissipation when flying at high altitude. Dealing with the traction drive, such challenges push for increasing the system voltage, which might reach tens of kV [5], thus achieving the target propulsion power while limiting the phase current. Nevertheless, the adoption of Medium Voltage (MV) drives introduce relevant design and control challenges, requiring multilevel converters [14]. At the meantime, multi-three-phase drives permit to further reduce the phase current while increasing the fault tolerance. In addition, achieving such high power density requirements necessitate a combined design of the drive and mechanical transmission, along with a broader optimization of the entire propulsion system.

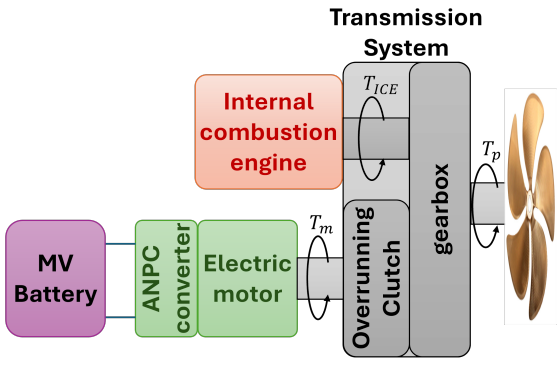

Fig. 1. System architecture.

Aviation systems must meet strict safety and reliability regulations, requiring high fault tolerance of motors [15], power converter [16], drive control strategies [17] and transmission system. Despite the motor behavior under symmetric short circuit can be predicted analytically [18], and mitigated through dedicated control strategies [19], reliable simulation models of the full system covering faulty conditions are essential for safety assessments, addressing electrical, thermal, and mechanical constraints at system level.

In this scenario, this work presents an integrated model of a MV electric drive and an overrunning clutch, designed for regional aircraft propulsion systems. The model is specifically tailored for the simulation of faulty conditions. The considered hybrid propulsion architecture is reported in Fig. 1, merging an Internal Combustion Engine (ICE) and a Medium Voltage (MV) drive within a dedicated transmission system. The transmission embeds an overrunning clutch, capable of disconnecting the drive from the propeller in the event of fault or in specific phases of the flight. The developed model covers torque and flux undulations due to space harmonics in three-phase and multi-phase drives, symmetric and asymmetric short circuits, open-phase faults, and switch failures in the power converter. Transient current and torque waveforms are computed, assessing risks such as motor overheating, demagnetization, torque/speed undulations on the transmission system and propeller, and potential clutch disengagement.

II. System Under Test and Simulation Model

A. Electric Motor and Control

The tested motor is a MV Permanent Magnet Synchronous Machine (PMSM) equipped with NdFeB magnets, designed for aerospace applications. The detailed geometry is covered by industrial property and cannot be disclosed here, but the motor ratings are reported in Tab. I. The high DC-link voltage (2400 V) permits the reduction of the phase current ratings despite the relevant continuous power requirements (810 kW). Two winding configurations are compared: a short-pitch 3-phase distributed winding and a full-pitch asymmetrical 6-phase winding. The former solution is the easiest solution for MV drives, while the latter allows phase current halving, reducing the inverter rating at the cost of a double inverter adoption [20], [21].

For each machine, 3D flux maps are computed with SyR-e [22] at the rated PM temperature. Thanks to the 3D maps, the harmonic content of torque and flux linkage is easily taken into account, with limited computational effort. In the developed simulation, the motor drive is modeled with a Controlled Current Generators (CCG) circuital approach. The corresponding block diagram is reported in Fig. 2 and is based on the pre-computed 3D flux maps, covering the effects of space harmonics [23]. A discrete-time field oriented control is implemented in a triggered subsystem, emulating the real drive operation.

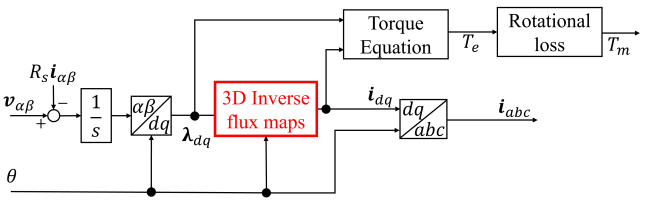

Fig. 2. Block diagram of the CCG motor model.

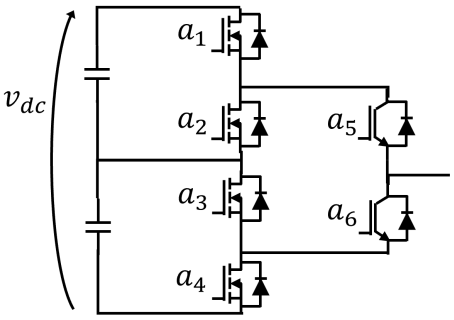

Fig. 3. Topology of the modeled ANPC [24].

B. Power Converter

A multi-level power converter is mandatory to deal with the rated DC-link voltage of 2400 V. Specifically, a 3-level Active Neutral-Point Clamped (ANPC) converter was adopted, combining Silicon Carbide (SiC) power MOSFETs with Si-based IGBTs [24]. The schematic of one leg of the converter, referred to phase a of the drive, is given in Fig. 3, also reporting the nomenclature adopted for each power switch. A dedicated modulation strategy is implemented [25] to minimize the commutation losses and the voltage steps on the machine, targeting maximum efficiency of the full drive.

The developed circuital model of the ANPC permits to emulate a fault in any of the converter switches separately, thus evaluating the consequences on the full propulsion system.

C. Transmission System and Overrunning Clutch

The overrunning clutch transmits torque between two components when engaged and allows free rotation in the opposite direction. Such clutches are widely used in helicopters and aircraft, where they play a critical role in their continued operation when one engine malfunctions, is shut down, or runs at a different speed from others [26]. In this context, the clutch

TABLE I
Ratings of the Drive

Peak torque	450 Nm
Max speed	19500 rpm
Base speed	17000 rpm
Continuous power	810 kW
Pole pairs	4
DC-link voltage	2400 V
Nominal phase current (3ph)	560 Apk
Nominal phase current (6ph)	280 Apk

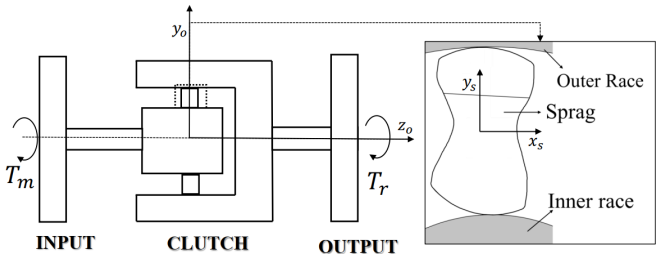

Fig. 4. Clutch model and sprags geometry.

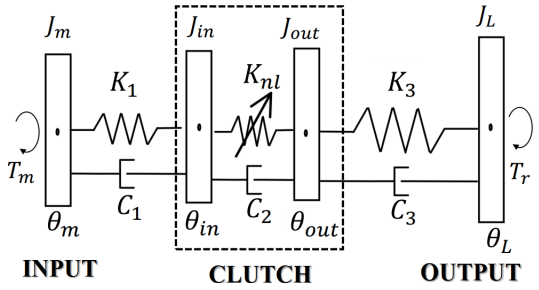

Fig. 5. Lumped parameter model of the overrunning clutch in Fig. 1.

is installed between the electrical drive and the gearbox. When disengaged, the drive is decoupled, allowing the turbo engine to power the propeller independently. The clutch engages again when needed (e.g., during cruise) to enable the drive to support the turbo engine.

Among the various types of overrunning clutches, the sprag clutch is commonly used in aviation applications due to its high overrunning speed capacity and superior reliability [27]. The sprag overrunning clutch shown in Fig. 4, consists of an inner race connected to the drive, an outer race connected to the gearbox, and sprags between them, allowing both freewheeling and engagement. The sprags are geometrically designed to wedge when the relative velocity between races is in the engaging direction, allowing torque transmission. In contrast, no torque is transmitted when the relative velocity corresponds to the disengaging direction.

The mechanical system is modeled as shown in Fig. 5, where the motor, races, and output are represented as rotational inertias, and the shafts are modeled using stiffness and damping elements. The sprags are represented by a piecewise nonlinear stiffness K_{nl}, which is zero when disengaged and becomes a nonlinear function of the relative rotational displacement between the races when engaged. The nonlinear engagement stiffness accounts for the increased deformation at the contact points based on Hertzian contact theory. The dynamic equations of motion of the system are as follows [28], [29]:

$$\mathbf{M}\ddot{\boldsymbol{\theta}}(t) + \mathbf{C}\dot{\boldsymbol{\theta}}(t) + \mathbf{K}\boldsymbol{\theta}(t) = \mathbf{T}_e(t) + \mathbf{T}_{NL}(t, \boldsymbol{\theta}, \dot{\boldsymbol{\theta}}) \quad (1)$$

The matrices $\mathbf{M}$, $\mathbf{C}$, and $\mathbf{K}$ represent the moment of inertia, torsional damping, and linear stiffness of the system, respectively. The external load vector $\mathbf{T}_e$ includes the moment from the electric motor, $T_m(t)$, and the aggregated moment on the output, $T_r(t)$, which results from the resistive moment on the propeller, $T_p(t)$, and the moment from the turbo engine, $T_{ICE}(t)$. The propeller imposes a quadratic resistive torque:

$$T_p(t) = C_p \dot{\theta}_L^2 \quad (2)$$

The moments $T_m(t)$ and $T_{ICE}(t)$ are defined based on the specific operating scenarios under investigation.

The vector $\mathbf{T}_{NL}(t, \boldsymbol{\theta}, \dot{\boldsymbol{\theta}})$ contains the state-dependent nonlinear moment T_c applied by the sprags to the inner and outer races. According to the defined piecewise nonlinear stiffness [28], [30], this moment is obtained as:

$$T_c = \begin{cases} 0 & \text{if } \dot{\theta}_{in} < \dot{\theta}_{out} \\ C_{te}|\theta_{in} - \theta_{out}|^{ne}(\theta_{in} - \theta_{out}) & \text{if } \dot{\theta}_{in} = \dot{\theta}_{out} \end{cases} \quad (3)$$

The exponent $ne = 0.5$ reflects the nonlinearity typical of point-contact interfaces, while the parameter $C_{te} = 2.152e4$ Nm/rad embeds the material and geometric properties of the interface.

III. Simulation Results

A. Short Circuit in the 3-phase machine

An example simulation in faulty conditions is reported in Fig. 6. This test is executed with the drive connected in 3-phase configuration. The MUT is torque controlled at the nominal torque (450 Nm) and rotating at the corner speed (17 krpm), while a 3-phase short circuit is triggered. This is the most dangerous pre-fault condition, inducing the highest transient current and torque [18]. The Figure reports the speed, torque, flux and current waveforms, permitting to numerically evaluate their peak values during the fault transient. The torque undulations visible before the fault event are due to the machine space harmonics, captured by the 3D $dq\theta$ flux maps.

In this specific fault scenario, the peak phase current magnitude and braking torque reach 1236 A and 524 Nm respectively. These values permit evaluating the risk of inverter or mechanical damages respectively, as a consequence of a 3-phase short circuit. In addition, the risk for PM demagnetization can be evaluated from the maximum negative transient current in d-axis, in this case equal to -1197 A. Moreover, the steady-state phase current can be estimated, thus evaluating potential thermal issues after fault. In this specific case, the steady-state current after fault is 396 A, i.e. lower than the nominal current, so it is thermally sustainable.

The transient current trajectory in the dq plane is reported in Fig. 7. Before the fault, the drive is correctly controlled on the MTPA locus. After the short circuit is triggered, the operating point rotates clockwise approximately along an iso-flux contour. The flux magnitude progressively reduces due to system losses (resistive voltage and rotational loss), so the operating point decades in a spiral before converging close to the characteristic current of the machine [18].

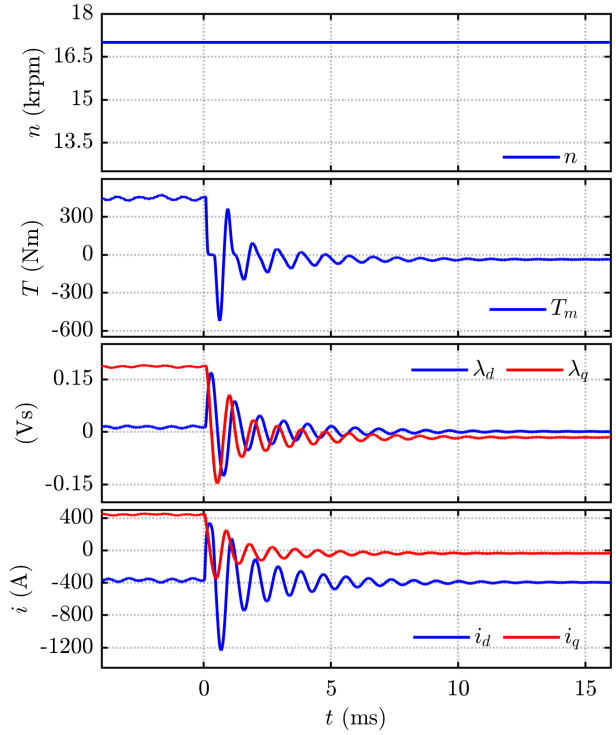

Fig. 6. 3-phase short-circuit fault in 3-phase drive configuration at the corner speed, nominal torque (17 krpm, 450 Nm). Torque, current and flux waveforms.

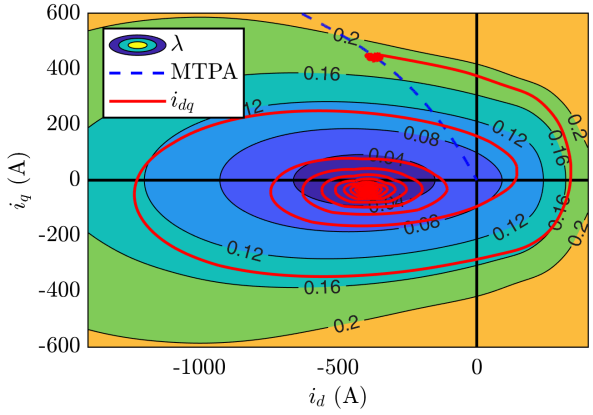

Fig. 7. 3-phase short-circuit fault in 3-phase drive configuration at the corner speed, nominal torque (17 krpm, 450 Nm). Current trajectory in the dq plane.

B. Short Circuit in the 6-phase machine

When dealing with multi-three-phase drives, a higher number of faulty scenario must be considered. This includes a 3-phase short circuit in each three-phase set, a phase-to-phase short between phases belonging to the same set and between phases of different sets. An example of results is reported

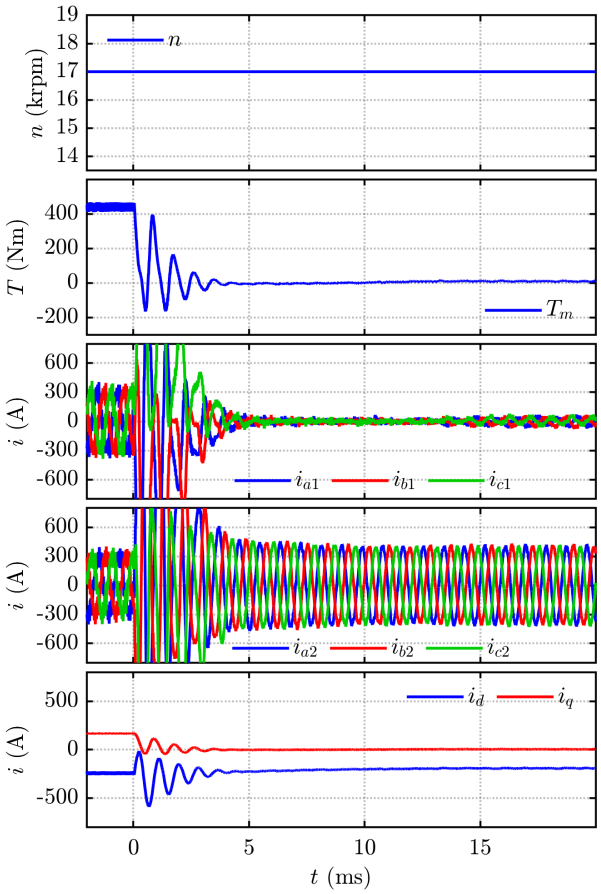

Fig. 8. 3-phase short-circuit fault of the set 1 in 6-phase drive configuration at the corner speed, nominal torque (17 krpm, 450 Nm).

in Fig. 8, referring to the drive in 6-phase configuration. The motor is again torque controlled at the nominal torque (450 Nm) while rotating at the base speed (17 krpm), when the first 3-phase set is shorted. During the short circuit, the second 3-phase set is still controlled aiming to maintain the reference torque.

Also for this fault condition, the simulation permits evaluating the transient torque and current per each 3-phase set. In this case, the presence of the second 3-phase set reduces the peak transient torque to -155 Nm. Anyway, the transient current is significantly higher compared to the 3-phase drive.

C. ANPC single switch fault

The developed model permits simulating faults on the ANPC power converter, to evaluate their effects on the electric machine and mechanical transmission system. An example is given in Fig. 9, simulating the failure in short circuit of the MOSFET a_1, i.e. the upper MOSFET of the leg a (see Fig. 3). The simulation refers again to the 3-phase drive configuration. The fault is simulated with the motor operating at 15 krpm, 400 Nm.

As can be noted, the 3-level converter is capable of maintaining the current control even if the MOSFET a_1

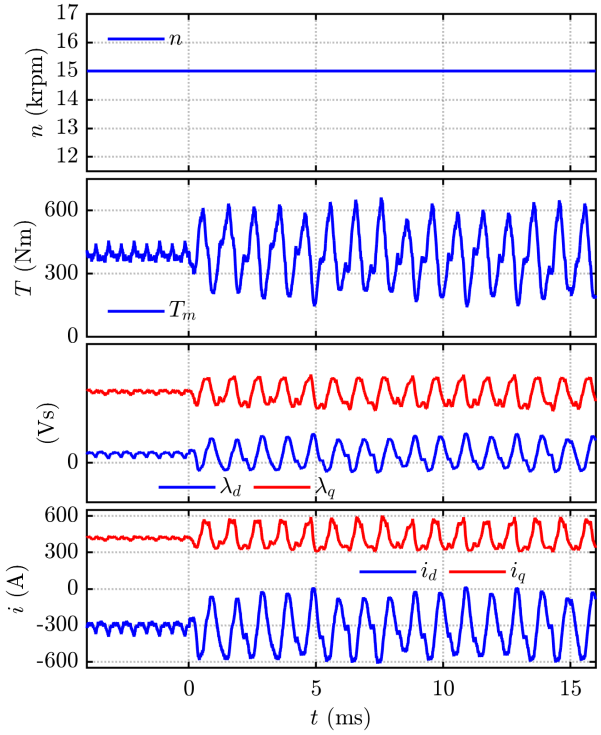

Fig. 9. Short-circuit failure of the MOSFET a_1 at 15 krpm, 400 Nm.

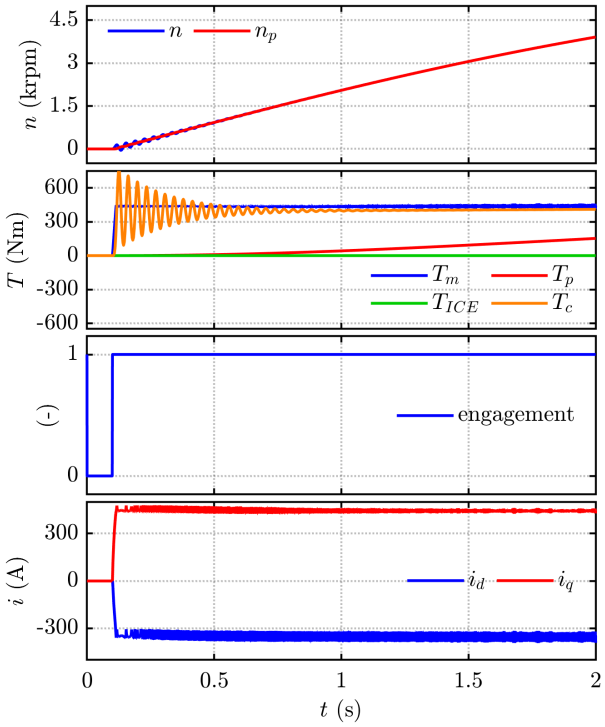

Fig. 10. Drive start-up at full torque (T_m=450 Nm) in the absence of T_{ICE}=0 Nm.

is permanently closes, thus maintaining the average torque to the reference T^*=400 Nm. This comes at the cost of relevant current and torque oscillations, correctly evaluated by the simulation model. Moreover, it should be noted that the balance between the two input capacitors of the ANPC is lost, with the lower capacitor in Fig. 3 charging above $v_{dc}/2$=1200 V. Therefore, a serious risk of subsequent failure of the other power switches is present.

D. Clutch Engagement

The dynamics of the mechanical transmission is evaluated, including the overrunning clutch, both in healthy and faulty conditions. A start-up transient is reported in Fig. 10, with the drive producing the nominal torque (450 Nm) and the ICE turned off. This test is meant for evaluating the starting capability of the drive. As can be noted, the clutch is suddenly engaged, permitting the acceleration of the electric motor and the propeller. Nevertheless, this engagement injects sufficient energy into the mechanical system in the engaged state to excite mechanical vibrations, resulting in oscillations in the torque transmitted by the clutch T_c (orange curve), computed according to (3). These oscillations, that can be mitigated by introducing higher damping into system, are reflected into speed bumps, visible in the motor speed n although damped by the large propeller inertia in the transmission output n_p. If these torque oscillations were excessively underdamped, with T_c approaching to zero, the clutch might disengage, thus resulting in an intermittent T_c during the start-up.

Finally, the effects of a 3-phase short circuit on the transmission system are depicted in Fig. 11. The simulation refers to a motor torque of 450 Nm, assisting the ICE torque of 600 Nm for rotating the propeller at 10 krpm, with the propeller imposing a resistive torque according to (2). As can be noted, after the short circuit the motor decelerates due to the fault braking torque, while the n_p decreases slowly due to the large inertia of the propeller and to the positive torque still produced by the ICE, partially compensating for the load T_p. This causes the clutch disengagement approximately 10.5 ms after the fault event, i.e. when θ_{in} becomes smaller than θ_{out} and contemporarily $\dot{\theta}_{in} < \dot{\theta}_{out}$, so the transmitted torque drops to zero. From there on, the speed dynamics of the motor is decoupled from the transmission, ICE and propeller.

IV. Conclusion

This work presents an accurate simulation model for a hybrid propulsion system in regional aircraft. The model is specifically developed for simulating faulty scenarios and evaluating their impact on the full propulsion system, assessing their impact on transmitted torque and propeller performance, as well as evaluating potential thermal and electromagnetic issues on the electric motor. The propulsion system features a medium-voltage drive reconfigurable as a 3-phase or 6-phase PMSM powered by an ANPC converter. The drive is coupled to the turbo engine and propeller via an overrunning clutch, enabling drive disengagement. The model covers both symmetric and asymmetric faults both in the motor and in the

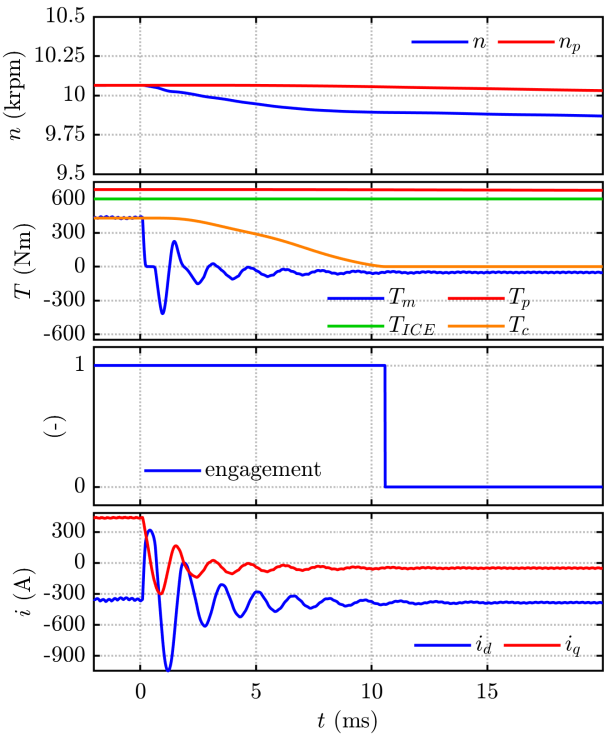

Fig. 11. 3-phase short circuit at 10 krpm, T_m=450 Nm, T_{ICE}=600 Nm, with consequent clutch disengagement.

ANPC converter, including single-switch faults, open circuits, and motor control reactions to the faults. The developed model is an useful tool for assessing the reliability and fault tolerance of aviation propulsion systems, which is of top importance for the developement of hybrid propulsion regional aircrafts.

ACKNOWLEDGMENT

The project is supported by the Clean Aviation Joint Undertaking and its members in the framework of Grant Agreement n° 101102020 - AMBER, funded by the European Union. Views and opinions expressed are however those of the author(s) only and do not necessarily reflect those of the European Union or Clean Aviation Joint Undertaking. Neither the European Union nor the granting authority can be held responsible for them.

The research was supported by the Power Electronics Innovation Center (PEIC) of Politecnico di Torino.

REFERENCES

[1] "InnovAtive deMonstrator for hyBrid-Electric Regional application (AMBER)," accessed: 2025-07-02. [Online]. Available: https://cordis.europa.eu/project/id/101102020

[2] B. Sarlioglu and C. T. Morris, "More electric aircraft: Review, challenges, and opportunities for commercial transport aircraft," *IEEE Transactions on Transportation Electrification*, vol. 1, no. 1, pp. 54–64, 2015.

[3] W. Cao, B. C. Mecrow, G. J. Atkinson, J. W. Bennett, and D. J. Atkinson, "Overview of electric motor technologies used for more electric aircraft (mea)," *IEEE Transactions on Industrial Electronics*, vol. 59, no. 9, pp. 3523–3531, 2012.

[4] J. Benzaquen, J. He, and B. Mirafzal, "Toward more electric powertrains in aircraft: Technical challenges and advancements," *CES Transactions on Electrical Machines and Systems*, vol. 5, no. 3, pp. 177–193, 2021.

[5] A. Barzkar and M. Ghassemi, "Components of electrical power systems in more and all-electric aircraft: A review," *IEEE Transactions on Transportation Electrification*, vol. 8, no. 4, pp. 4037–4053, 2022.

[6] C. Gu, H. Yan, J. Yang, G. Sala, D. De Gaetano, X. Wang, A. Galassini, M. Degano, X. Zhang, and G. Buticchi, "A multiport power conversion system for the more electric aircraft," *IEEE Transactions on Transportation Electrification*, vol. 6, no. 4, pp. 1707–1720, 2020.

[7] Y. Ji, P. Giangrande, H. Zhao, W. Zhao, V. Madonna, H. Zhang, and M. Galea, "Electrical machine design considering corona-resistant wire for more electric aircraft applications," *IEEE Transactions on Transportation Electrification*, vol. 9, no. 2, pp. 3192–3202, 2023.

[8] E. Sayed, M. Abdalmagid, G. Pietrini, N.-M. Sa'adeh, A. D. Callegaro, C. Goldstein, and A. Emadi, "Review of electric machines in more-/hybrid-/turbo-electric aircraft," *IEEE Transactions on Transportation Electrification*, vol. 7, no. 4, pp. 2976–3005, 2021.

[9] M. Villani, F. Parasiliti, M. Tursini, G. Fabri, and L. Castellini, "Pm brushless motors comparison for a fenestron®type helicopter tail rotor," in *2016 International Symposium on Power Electronics, Electrical Drives, Automation and Motion (SPEEDAM)*, 2016, pp. 22–27.

[10] C. Gerada and K. J. Bradley, "Integrated pm machine design for an aircraft EMA," *IEEE Transactions on Industrial Electronics*, vol. 55, no. 9, pp. 3300–3306, 2008.

[11] J. Chen, C. Wang, and J. Chen, "Investigation on the selection of electric power system architecture for future more electric aircraft," *IEEE Transactions on Transportation Electrification*, vol. 4, no. 2, pp. 563–576, 2018.

[12] F. Stella, S. Savio, E. Vico, R. Bojoi, and E. Armando, "Cost effective 3d printed heatsink for fast prototyping of wbg power converters," in *2024 IEEE Applied Power Electronics Conference and Exposition (APEC)*, 2024, pp. 2562–2567.

[13] P. Pescetto, A. Sierra-Gonzalez, F. Alvarez-Gonzalez, H. Kapeller, E. Trancho, and G. Pellegrino, "Active control of variable dc-link for maximum efficiency of traction motor drives," *IEEE Transactions on Industry Applications*, vol. 59, no. 4, pp. 4120–4129, 2023.

[14] J. He, Q. Yang, and Z. Wang, "On-line fault diagnosis and fault-tolerant operation of modular multilevel converters — a comprehensive review," *CES Transactions on Electrical Machines and Systems*, vol. 4, no. 4, pp. 360–372, 2020.

[15] X. Jiang, D. Xu, L. Gu, Q. Li, B. Xu, and Y. Li, "Short-circuit fault-tolerant operation of dual-winding permanent-magnet motor under the four-quadrant condition," *IEEE Transactions on Industrial Electronics*, vol. 66, no. 9, pp. 6789–6798, 2019.

[16] F. Stella, O. Olanrewaju, Z. Yang, A. Castellazzi, and G. Pellegrino, "Experimentally validated methodology for real-time temperature cycle tracking in sic power modules," *Microelectronics Reliability*, vol. 88-90, pp. 615–619, 2018.

[17] M. Salehifar, R. S. Arashloo, J. M. Moreno-Equilaz, V. Sala, and L. Romeral, "Fault detection and fault tolerant operation of a five phase pm motor drive using adaptive model identification approach," *IEEE Journal of Emerging and Selected Topics in Power Electronics*, vol. 2, no. 2, pp. 212–223, 2014.

[18] S. Ferrari, G. Dilevrano, P. Ragazzo, P. Pescetto, and G. Pellegrino, "Fast determination of transient short-circuit current of pm synchronous machines via magnetostatic flux maps," *IEEE Transactions on Industry Applications*, vol. 59, no. 4, pp. 4000–4009, 2023.

[19] G. F. Olson, A. Bojoi, P. Pescetto, S. Ferrari, L. Peretti, and G. Pellegrino, "Active short-circuit strategy for PMSMs enabling bounded transient torque and demagnetization current," *IEEE Access*, vol. 12, pp. 109 001–109 011, 2024.

[20] E. Levi, "Multiphase electric machines for variable-speed applications," *IEEE Transactions on Industrial Electronics*, vol. 55, no. 5, pp. 1893–1909, 2008.

[21] M. Zhang, M. Yuan, and J. Jiang, "A comprehensive review of the multiphase motor drive topologies for high-power electric vehicle: Current status, research challenges, and future trends," *IEEE Transactions on Transportation Electrification*, vol. 11, no. 1, pp. 3631–3654, 2025.

[22] Simone Ferrari and Gianmario Pellegrino, "SyR-e: Synchronous reluctance - evolution." [Online]. Available: https://github.com/SyR-e/syre$_public$

[23] A. Varatharajan, D. Brunelli, S. Ferrari, P. Pescetto, and G. Pellegrino, "syredrive: Automated sensorless control code generation for

synchronous reluctance motor drives," in *2021 IEEE Workshop on Electrical Machines Design, Control and Diagnosis (WEMDCD)*, 2021, pp. 192–197.

[24] D. Zhang, J. He, and D. Pan, "A megawatt-scale medium-voltage high-efficiency high power density "sic+si" hybrid three-level anpc inverter for aircraft hybrid-electric propulsion systems," *IEEE Transactions on Industry Applications*, vol. 55, no. 6, pp. 5971–5980, 2019.

[25] D. Zhang, J. He and D. Pan, "A megawatt-scale medium-voltage high efficiency high power density "SiC+Si" hybrid three-level anpc inverter for aircraft hybrid-electric propulsion systems," in *2018 IEEE Energy Conversion Congress and Exposition (ECCE)*, 2018, pp. 806–813.

[26] P. Lynwander, A. Meyer, and S. Chachakis, "Sprag overriding aircraft clutch - performance of high speed overriding clutch assemblies for helicopters - [final report, 15 mar.- 15 dec. 1971]."

[27] Y. Xue, Z. Wang, D. Chen, S. Tao, and Y. Lu, "Design and test of a new type of overrunning clutch," *Machines*, vol. 10, no. 12, p. 1188, 2022.

[28] T. Xu and G. Lowen, "A mathematical model of an over-running sprag clutch," *Mechanism and machine theory*, vol. 29, no. 1, pp. 11–23, 1994.

[29] C. Huang, Y. Zhao, M. Liu, and Z. Fu, "Dynamic modelling and vibration analysis of dual-rotor system with inter-shaft sprag clutch and bearings," in *ICEMS2019*.

[30] Z.-h. Liu, H.-z. Yan, and Y.-m. Cao, "Design and analysis of logarithmic spiral type sprag one-way clutch," *Journal of Central South University*, vol. 22, no. 12, pp. 4597–4607, 2015.